Viscoacoustic model for near-field ultrasonic levitation

Ivan Melikhov*
Corning Scientific Center, 26A Shatelena Str., Saint Petersburg, 194021, Russia
and ITMO University, 49 Kronverksky Pr., Saint Petersburg, 197101, Russia

Sergey Chivilikhin
ITMO University, 49 Kronverksky Pr., Saint Petersburg, 197101, Russia

Alexey Amosov
Corning Scientific Center, 26A Shatelena Str., Saint Petersburg, 194021, Russia

Romain Jeanson
Corning European Technology Center, 7bis, Avenue de Valvins, 77210 Avon, France
(Received 27 May 2016; published 4 November 2016)

Ultrasonic near-field levitation allows for contactless support and transportation of an object over vibrating surface. We developed an accurate model predicting pressure distribution in the gap between the surface and levitating object. The formulation covers a wide range of the air flow regimes: from viscous squeezed flow dominating in small gap to acoustic wave propagation in larger gap. The paper explains derivation of the governing equations from the basic fluid dynamics. The nonreflective boundary conditions were developed to properly define air flow at the outlet. Comparing to direct computational fluid dynamics modeling our approach allows achieving good accuracy while keeping the computation cost low. Using the model we studied the levitation force as a function of gap distance. It was shown that there are three distinguished flow regimes: purely viscous, viscoacoustic, and acoustic. The regimes are defined by the balance of viscous and inertial forces. In the viscous regime the pressure in the gap is close to uniform while in the intermediate viscoacoustic and the acoustic regimes the pressure profile is wavy. The model was validated by a dedicated levitation experiment and compared to similar published results.

DOI: 10.1103/PhysRevE.94.053103

I. INTRODUCTION

The acoustic levitation is a phenomenon when an object is suspended in acoustic field. There are two different types of such levitation. The first one is usually associated with suspension of small particles placed between an acoustic actuator and reflector. The second type is denoted to the case when a levitating object has larger size and the distance between the object and an actuator is much smaller than the acoustic wavelength. Since high-frequency sound is usually used, the last type is often called ultrasonic near-field levitation.

The last type is used in manufacturing of highly precise products, such as silicon wafers of semiconductors, when contactless transportation system or suspension is needed. The phenomenon of ultrasonic near-filed levitation was first reported by Salbu [1]. A number of experimental and theoretical works have been published in recent years. Transportation system based on the flexural traveling waves of a vibrating substrate were examined by Hashimoto *et al.* [2,3]. Different system configuration was considered, including two-rails systems [4] and V-shaped rails [5]. Another approach is offered by Yoshimoto *et al.* [6,7], who suggest a slider with vibration source floating over a linear guideway. In addition, motor with levitated rotor [8], ultrasonic clutch [9], and journal bearing systems [10,11] were investigated.

The theory of acoustic radiation pressure in inviscid fluid was first described by Lord Rayleigh [12,13]. After that, there were many confusions until the work of Chu and Apfel [14], who accurately posed the question on the acoustic pressure and carried out one-dimensional analysis from the very basics. Later, Lee and Wang [15] extended their approach to higher dimensions. Their results were used for estimation of the levitation force in Refs. [2–4,8,9]. Although this approach allows fast computation of the force, it is inaccurate for small levitation distances.

When a system involves length scale comparable to the acoustic boundary layer thickness, viscous effects should be taken into account. In the case of particle levitation, the theory was extended to viscous fluids (see, for example, Ref. [16]), thermoviscous effects were incorporated [17], particle movement [18], and its elastic behavior [19] were studied. Regarding near-field levitation, it is common to suggest a very small gap thickness and purely viscous flow. To solve such problems different methods can be applied. For example, the approach described in Ref. [20] can be adopted in order to compute the pressure propagation into a long thin layer of gas. On the other hand, many researches employ well-known nonlinear Reynolds equation for a lubrication layer. It assumes that due to small gap thickness the inertia effects are negligibly small comparing to the viscous ones (for more details on lubrication theory, see, for example, Ref. [21]). This approach is used in Refs. [6,7,11]. Minikes and Bucher [22] utilized Reynolds equation coupled with elastic analysis of the ultrasonic actuator. In Ref. [23] the Reynolds equation was simplified with the help of perturbation theory. Later, Ilssar and Bucher [24] used it to examine motion of a levitating object. However, in spite of simplicity, the

*melikhovif@corning.com

lubrication approach is limited to the cases of extremely small levitation distances of the order of boundary layer thickness.

In practice, the weight of a suspended object is known in advance, the levitation distance is not. Therefore, there is no criteria if acoustic or viscous model should be used. In addition, at moderate distances an intermediate viscoacoustic regime appears, which is not resolved by these approaches. Thus, more general model is highly appreciated.

There are a number of numerical studies of transient Navier-Stokes system. In the work of Nomura *et al.* [25] a numerical solution shows excellent agreement with experimental data, while the simplest acoustic model gives inaccurate results. A similar numerical study was made by Minikes and Bucher [26] and compared to the lubrication model, which predicts larger levitation force. Both numerical studies use nontrivial computation schemes with nonreflective boundary conditions on the outer boundaries. Although a full numerical study is the most accurate one, it lacks speed of computation and hardly can be used in real-time control systems.

The mentioned above problem of well-posed boundary conditions at the end of the gap is important for the acoustic pressure computation. Turns [27] offered a semiempirical approach to compute the pressure drop at the edge of bearing film. Later, Li *et al.* [28] suggested an approximated boundary condition on the pressure drop. However, their approach is applied for incompressible fluids, which is not accurate for the case of acoustics.

In this paper we propose a semianalytical approach that allows us to cover viscous, acoustic, and intermediate viscoacoustic levitation regimes in a natural way. The developed mathematical model can be applied for a wide range of levitation heights, which is confirmed by experiment.

In the first section we describe the model's assumptions and theoretical background, starting from very general gas flow equations. We show the derivation of nonreflective boundary conditions on pressure as well. Next we overview numerical implementation and briefly describe the experiment, which was conducted to validate the theory. Finally, we provide the comparison of our model to the model and experimental data published in Ref. [25] and our experiment, then give qualitative results on the pressure distribution in the gap.

II. THEORY OF THE AIR FLOW

In this section we derive the governing equations of the air flow in the gap between actuator and levitating object. First of all, the basic equations are written out. Its formulation is based on the textbook of Landau and Lifshitz [29]. Then we make scaling analysis, which helps to determine the significant terms. After that we introduce a small parameter, the ratio between the vibration amplitude and the levitation height, and focus on the periodic solutions only. In the end of this section we describe nonreflective boundary conditions.

A. Governing equation

Although we focus on the levitation of a disk, the equations will be obtained in Cartesian coordinates, so the model can be applied to nonaxisymmetric geometry.

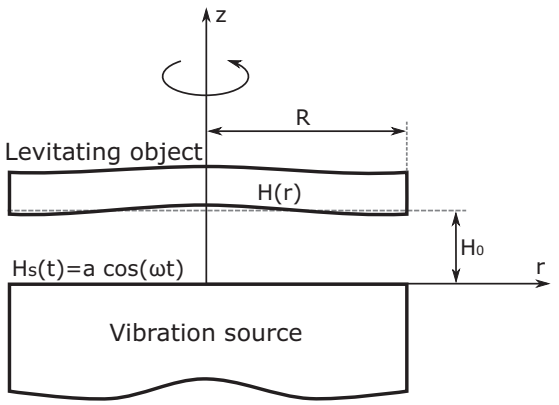

FIG. 1. Ultrasonic levitation of a disk.

Consider a planar ultrasonic source with the vibration amplitude a and the circular frequency ω. In the sake of simplicity, we assume its displacement depends only on time:

$$H_s(t) = a\cos(\omega t). \tag{1}$$

Nevertheless, treating the spatial dependence for modeling flexural vibrating surfaces requires only minor changes in the further theory.

The axes x_1 and x_2 are chosen to lie along the vibrating plane and the axis $z = x_3$ is perpendicular to the plane. We use Latin indices (such as in x_i or x_j) to span the numbers 1,2,3. Einstein's summation convention for repeated indices is used as well.

The levitation object is assumed to be motionless and its bottom surface can be slightly nonplanar (due to small deformations, for example). Its shape is described by a smooth function $H(x_1,x_2)$. The average levitation height is denoted by H_0. We do not consider here surface roughness and corresponding effects, such as scattering of acoustic waves.

The total gap thickness can be calculated by

$$h(t,x_1,x_2) = H(x_1,x_2) - H_s(t). \tag{2}$$

Figure 1 illustrates the levitation of a disk in the axysimmetric case (here $r = \sqrt{x_1^2 + x_2^2}$).

We start with the Navier-Stokes equations for compressible gas:

$$\rho(\partial_t \boldsymbol{v} + (\boldsymbol{v}\cdot\nabla)\boldsymbol{v}) = \nabla\cdot\boldsymbol{\sigma}, \tag{3a}$$

$$\partial_t\rho + \nabla\cdot(\rho\boldsymbol{v}) = 0, \tag{3b}$$

where ρ is the gas density, $\boldsymbol{v} = (v_{x_1}, v_{x_2}, v_z)$ is the velocity vector, and $\boldsymbol{\sigma}$ is the stress tensor given by

$$\boldsymbol{\sigma} = -p\boldsymbol{I} + \boldsymbol{\tau}, \tag{4}$$

where $\boldsymbol{I}$ is the unit tensor, p is the pressure, and viscous stress tensor $\boldsymbol{\tau}$ is defined as

$$\boldsymbol{\tau} = \mu[\nabla\boldsymbol{v} + (\nabla\boldsymbol{v})^T] + \left(\mu^b - \tfrac{2}{3}\mu\right)(\nabla\cdot\boldsymbol{v})\boldsymbol{I}, \tag{5}$$

where μ is the dynamic viscosity, and μ^b is the bulk viscosity.

The dynamics equations are accompanied by the energy equation

$$\rho T(\partial_t s + \boldsymbol{v}\cdot\nabla s) = \nabla\cdot(\kappa\nabla T) + \Phi, \tag{6}$$

where T is the air temperature, s is the entropy, κ is the thermal conductivity of the gas, Φ is the viscous dissipation term, in Cartesian coordinates given by

$$\Phi = \tau_{ik}\frac{\partial v_i}{\partial x_k}.$$

We take into account the viscosity-temperature dependence in the same way as in Ref. [25], by assuming semiempirical Sutherland's law [30],

$$\mu = \mu_0\left(\frac{T}{T_0}\right)^{3/2}\frac{T_0 + C}{T + C}, \tag{7}$$

where μ_0, T_0, and C are empirical constants.

We assume that the gas pressure, density, and temperature are coupled by the ideal gas law,

$$p = \rho\frac{\mathcal{R}}{\mathcal{M}}T, \tag{8}$$

where $\mathcal{R}$ is the universal gas constant and $\mathcal{M}$ is the molar mass of gas.

The levitation force can be found by integrating the vertical component of the stress tensor σ_{zz} over the object's surface:

$$F = -\iint (\sigma_{zz}|_{z=H})\,dx_1\,dx_2, \tag{9}$$

where

$$\sigma_{zz} = -p + \mu\left[2\frac{\partial v_z}{\partial z} + \left(\mu^b - \frac{2}{3}\mu\right)\nabla\cdot\boldsymbol{v}\right]. \tag{10}$$

B. Scaling analysis

In this section we carry out scaling analysis in order to neglect small terms. Let's introduce the longitudinal and transversal length scales, disk radius R, and average gap thickness H_0, respectively, and the timescale ω^{-1}. Although it is natural to choose the transversal velocity scale equal to the vibrating wall speed $a\omega$, it is more convenient to take it as ωH_0, as a common choice in the lubrication theory. The longitudinal velocity scale U is chosen to keep the continuity equation terms of the same scale, then $U = \omega R$. The nondimensional variables are

$$\tilde{x}_\alpha = \frac{x_\alpha}{R}, \quad \tilde{z} = \frac{z}{H_0}, \quad \tilde{t} = \omega t, \quad \tilde{v}_z = \frac{v_z}{\omega H_0}, \quad \tilde{v}_\alpha = \frac{v_\alpha}{\omega R},$$
$$\tilde{p} = \frac{p}{p_0}, \quad \tilde{\rho} = \frac{\rho}{\rho_0}, \quad \tilde{\mu} = \frac{\mu}{\mu_0}, \quad \tilde{s} = \frac{s}{c_v}, \quad \tilde{T} = \frac{T}{T_0},$$

where c_v is the heat capacity at constant volume and p_0, ρ_0, μ_0, T_0 are the pressure, density, viscosity, and temperature of air at normal conditions; index α spans the numbers 1–2.

The scaling analysis is based on the following assumptions:

(1) the gap thickness is much smaller than the acoustic wavelength λ, $H_0 \ll \lambda$;

(2) the gap thickness is much smaller than its length, $H_0 \ll R$;

(3) the vibration amplitude is much smaller than the gap thickness, $a \ll H_0$.

In the case of the near-field levitation, the first two assumptions are always held. The last assumption will be used to introduce a small parameter to the model. The details of scaling analysis can be found in the Appendix.

First, we treat the energy Eq. (6). As shown in the Appendix, this equation can be reduced to

$$\partial_{\tilde{t}}\tilde{s} + \tilde{\boldsymbol{v}}\cdot\tilde{\boldsymbol{\nabla}}\tilde{s} = 0, \tag{11}$$

where $\tilde{\boldsymbol{\nabla}}$ is a nondimensional nabla operator. We assume that at the initial time the entropy is constant. Together with Eq. (11) it implies that the entropy remains constant during the process. Using the expression for the entropy of ideal gas (nondimensional),

$$\tilde{s} = \ln\left(\frac{\tilde{p}}{\tilde{\rho}^\gamma}\right), \tag{12}$$

we conclude that the process is adiabatic, which is common in acoustics, and obtain the relation between the nondimensional density and pressure,

$$\tilde{\rho} = \tilde{p}^{1/\gamma}, \tag{13}$$

where γ is the adiabatic index. Then, using Eqs. (7), (8), and (13), we can express the nondimensional viscosity in terms of pressure:

$$\tilde{\mu} = \frac{T_0 + C}{T_0}\frac{\tilde{p}^{(3-3/\gamma)/2}}{\tilde{p}^{1-1/\gamma} + C/T_0}. \tag{14}$$

For further analysis, it is vital to split the velocities in the longitudinal and transversal directions: $\tilde{\boldsymbol{u}} = (\tilde{v}_{x_1}, \tilde{v}_{x_2})$ and $\tilde{v}_z$. Considering the different components of the governing Eqs. (3a) and (3b) and taking into account the assumptions 1–3 above, we can neglect small terms and simplify the equations (see Appendix for details):

$$\partial_{\tilde{z}}\tilde{p} = 0, \tag{15a}$$
$$\gamma K^2\tilde{\rho}(\partial_{\tilde{t}}\tilde{\boldsymbol{u}} + (\tilde{\boldsymbol{v}}\cdot\tilde{\boldsymbol{\nabla}}\tilde{\boldsymbol{u}})) = -\tilde{\boldsymbol{\nabla}}_{\boldsymbol{s}}\tilde{p} + \Sigma\partial_{\tilde{z}}(\tilde{\mu}\partial_{\tilde{z}}\tilde{\boldsymbol{u}}), \tag{15b}$$
$$\partial_{\tilde{t}}\tilde{\rho} + \tilde{\boldsymbol{\nabla}}\cdot(\tilde{\rho}\tilde{\boldsymbol{v}}) = 0, \tag{15c}$$

where $K^2 = \omega^2R^2\gamma^{-1}\rho_0/p_0$ is the squared nondimensional acoustic wave number, and $\Sigma = \mu_0\omega R^2/(p_0H_0^2)$ is so-called "squeeze number" (in the lubrication theory, see Ref. [21], squeeze number is refereed to 12Σ); $\tilde{\boldsymbol{\nabla}}_{\boldsymbol{s}}$ acts on the coordinates $\tilde{x}_1$, $\tilde{x}_2$ only.

During the derivation of the Reynolds equation for viscous flow K is assumed to be negligible (for derivation of the equation see Ref. [21]), while linear acoustic does not account the term multiplied by Σ (see Refs. [14,15]). In our study we keep both terms, thus taking into account viscous and inertial (acoustic) effects.

Equation (15a) means that the pressure does not vary through the gap thickness. It implies that the density [see Eq. (13)] and the viscosity [see Eq. (14)] are constant through thickness as well. Further, we consider the pressure, density, and viscosity to be independent on z coordinate.

As shown in the Appendix, scaling analysis allows simplifying the normal stress to the form

$$\tilde{\sigma}_{\tilde{z}\tilde{z}} = -\tilde{p}. \tag{16}$$

Thus, the levitation force can be calculated as an integral of pressure:

$$\tilde{F} = -\iint \tilde{\sigma}_{\tilde{z}\tilde{z}}|_{\tilde{z}=\tilde{H}}\,d\tilde{x}_1\,d\tilde{x}_2 = \iint \tilde{p}\,d\tilde{x}_1\,d\tilde{x}_2. \tag{17}$$

The equations must be equipped with the no-slip boundary conditions:

$$\tilde{\boldsymbol{u}}|_{\tilde{z}=\tilde{H}_s} = \tilde{\boldsymbol{u}}|_{\tilde{z}=\tilde{H}} = 0, \tag{18a}$$

$$\tilde{v}_z|_{\tilde{z}=\tilde{H}_s} = -\partial_{\tilde{t}}\tilde{h} = -a/H_0 \sin(\tilde{t}), \quad \tilde{v}_z|_{\tilde{z}=\tilde{H}} = 0. \tag{18b}$$

C. Averaging over the gap thickness

Starting from here we denote the nondimensional variables without a tilde for clarity.

Before going further, we average the continuity Eq. (15c) by integrating it with respect to z coordinate from $H_s(t)$ to $H(x_1,x_2)$ and dividing by $h(t,x_1,x_2)$. Note that according to Eq. (15a) the averaged pressure, density, and viscosity are equal to the nonaveraged ones:

$$\bar{p} = p, \quad \bar{\rho} = \rho, \quad \bar{\mu} = \mu. \tag{19}$$

Integrating Eq. (15c), applying the rule of integral differentiation and taking into account boundary conditions Eq. (18), one gets

$$\partial_t(\rho h) + \nabla_s \cdot (\rho h \bar{\boldsymbol{u}}) = 0, \tag{20}$$

where the gap-averaged velocity is given by

$$\bar{\boldsymbol{u}} = \frac{1}{h}\int_{H_s}^{H} \boldsymbol{u}\, dz. \tag{21}$$

Equation (20) with the equations of dynamics Eq. (15b), the density-pressure dependence Eq. (13), and the viscosity-pressure dependence Eq. (14) may be used to compute the pressure profile. However, despite neglecting pressure dependence on z coordinate, these equations are still nonlinear and time-dependent. Further simplification may be obtained by asymptotic analysis described in the next section.

D. Asymptotic analysis

Here we introduce the parameter $\varepsilon = a/H_0$, the ratio between the vibration amplitude and the gap thickness, which is small for the most experimental cases. We are going to find the series solution in the form

$$\begin{aligned}
\rho &= 1 + \varepsilon\rho^{(1)} + \varepsilon^2\rho^{(2)} + O(\varepsilon^3),\\
p &= 1 + \varepsilon p^{(1)} + \varepsilon^2 p^{(2)} + O(\varepsilon^3),\\
\mu &= 1 + \varepsilon\mu^{(1)} + \varepsilon^2\mu^{(2)} + O(\varepsilon^3),\\
\boldsymbol{u} &= \boldsymbol{0} + \varepsilon\boldsymbol{u}^{(1)} + \varepsilon^2\boldsymbol{u}^{(2)} + O(\varepsilon^3),\\
v_z &= 0 + \varepsilon v_z^{(1)} + \varepsilon^2 v_z^{(2)} + O(\varepsilon^3),\\
h &= h^{(0)}(x_1,x_2) + \varepsilon h^{(1)}(t), \quad h^{(1)}(t) = -\cos(t),
\end{aligned}$$

where $h^{(0)}(x_1,x_2) = H(x_1,x_2)/H_0$.

Using the relationship Eqs. (13) and (14) we write out the density terms,

$$\rho^{(1)} = \frac{1}{\gamma}p^{(1)}, \quad \rho^{(2)} = \frac{1}{\gamma}p^{(2)} - \frac{\gamma-1}{2\gamma^2}(p^{(1)})^2, \tag{22}$$

and the viscosity term,

$$\mu^{(1)} = \frac{(\gamma-1)}{2\gamma}\frac{T_0+3C}{T_0+C}p^{(1)} = Mp^{(1)}. \tag{23}$$

Substituting the series into the continuity Eq. (20) and collecting the terms of the same order, we get

$$\partial_t\left(\frac{h^{(0)}p^{(1)}}{\gamma}\right) + \nabla_s \cdot (h^{(0)}\bar{\boldsymbol{u}}^{(1)}) = -\partial_t h^{(1)} \tag{24}$$

for the first order, and

$$\begin{aligned}
&\partial_t\left(\frac{h^{(0)}p^{(2)}}{\gamma}\right) + \nabla_s \cdot (h^{(0)}\bar{\boldsymbol{u}}^{(2)})\\
&\quad = -\partial_t\left[\frac{h^{(1)}p^{(1)}}{\gamma} - \frac{\gamma-1}{2\gamma^2}h^{(0)}(p^{(1)})^2\right]\\
&\qquad - \nabla_s \cdot \left[\left(\frac{h^{(0)}p^{(1)}}{\gamma} + h^{(1)}\right)\bar{\boldsymbol{u}}^{(1)}\right]
\end{aligned} \tag{25}$$

for the second order.

To find the averaged velocity we need to solve Eqs. (15b). For the first order it takes the form

$$\gamma K^2 \partial_t \boldsymbol{u}^{(1)} = -\nabla_s p^{(1)} + \Sigma\partial_{zz}^2\boldsymbol{u}^{(1)}, \tag{26a}$$

$$\boldsymbol{u}^{(1)}|_{z=0} = 0, \quad \boldsymbol{u}^{(1)}|_{z=h^{(0)}} = 0, \tag{26b}$$

$$\bar{\boldsymbol{u}}^{(1)} = \frac{1}{h^{(0)}}\int_0^{h^{(0)}} \boldsymbol{u}^{(1)}\, dz, \tag{26c}$$

and for the second order the equations are

$$\begin{aligned}
&\gamma K^2[\partial_t\boldsymbol{u}^{(2)} + \gamma^{-1}p^{(1)}\partial_t\boldsymbol{u}^{(1)} + (\boldsymbol{v}^{(1)}\cdot\nabla)\boldsymbol{u}^{(1)}]\\
&\quad = -\nabla_s p^{(2)} + \Sigma\left(\partial_{zz}^2\boldsymbol{u}^{(2)} + Mp^{(1)}\partial_{zz}^2\boldsymbol{u}^{(1)}\right),
\end{aligned} \tag{27a}$$

$$\boldsymbol{u}^{(2)}|_{z=0} = h^{(1)}\partial_z\boldsymbol{u}^{(1)}, \quad \boldsymbol{u}^{(2)}|_{z=h^{(0)}} = 0, \tag{27b}$$

$$\bar{\boldsymbol{u}}^{(2)} = \frac{1}{h^{(0)}}\int_0^{h^{(0)}} \boldsymbol{u}^{(2)}\, dz - \frac{h^{(1)}}{h^{(0)}}\bar{\boldsymbol{u}}^{(1)}. \tag{27c}$$

The transversal velocity $v_z^{(1)}$, which is included in the inertial term, can be obtained from the continuity Eq. (15c):

$$v_z^{(1)} = -\int_0^z (\gamma^{-1}\partial_t p^{(1)} + \nabla_s \cdot \boldsymbol{u}^{(1)})\, dz' - \partial_t h^{(1)}. \tag{28}$$

E. Periodic solution

We focus on the steady state, when a suspended object is motionless, and we may be interested only in stationary solution. However, the only driving cause of the flow is periodic vibration and stationary pressure may be generated by nonlinear effects exclusively. It is natural to look for the solution in form of Fourier series with the base frequency of the transducer's vibration (which is equal to 1 in nondimensional form):

$$p^{(m)} = \sum_{n=1}^{\infty} p_n^{(m)} e^{int}, \quad \boldsymbol{u}^{(m)} = \sum_{n=1}^{\infty} \boldsymbol{u}_n^{(m)} e^{int},$$

$$h^{(1)} = \sum_{n=1}^{\infty} h_n^{(1)} e^{int} = -\cos(t) = -\frac{1}{2}(e^{it} + e^{-it}).$$

Substituting the series into the first-order Eqs. (24), (26), and (28) implies the equation on pressure,

$$\frac{in}{\gamma}h^{(0)}p_n^{(1)} + \nabla_s \cdot \left(h^{(0)}\bar{\boldsymbol{u}}_n^{(1)}\right) = -inh_n^{(1)}, \tag{29}$$

the equation on longitudinal velocity,

$$\mathrm{i}n\gamma K^2 \boldsymbol{u}_n^{(1)} = -\nabla_s p_n^{(1)} + \Sigma \partial_{zz}^2 \boldsymbol{u}_n^{(1)}, \tag{30a}$$

$$\boldsymbol{u}_n^{(1)}\big|_{z=0} = 0, \quad \boldsymbol{u}_n^{(1)}\big|_{z=h^{(0)}} = 0, \tag{30b}$$

$$\bar{\boldsymbol{u}}_n^{(1)} = \frac{1}{h^{(0)}} \int_0^{h^{(0)}} \boldsymbol{u}_n^{(1)}\, dz, \tag{30c}$$

and the expression for the transversal velocity,

$$v_{zn}^{(1)} = -\int_0^z \left(\frac{\mathrm{i}n}{\gamma} p_n^{(1)} + \nabla_s \cdot \boldsymbol{u}_n^{(1)} \right) dz' - \mathrm{i}n h_n^{(1)}. \tag{31}$$

To find the steady levitation force we need a time-independent solution for pressure, i.e., for $n = 0$. However, nontrivial solutions of Eqs. (29) and (30) exist only for $n = \pm 1$. It implies zero time-averaged pressure. Thus, we have to study the second-order equations.

Substituting the series into Eqs. (25) and (27) we get the equation on zero-harmonic quantities:

$$\nabla_s \cdot \left(h^{(0)} \bar{\boldsymbol{u}}_0^{(2)} \right) = -\nabla_s \cdot \left[\left(\frac{h^{(0)} p^{(1)}}{\gamma} + h^{(1)} \right) \bar{\boldsymbol{u}}^{(1)} \right]_0, \tag{32}$$

and

$$\mathrm{i}K^2 \left[n p_n^{(1)} \boldsymbol{u}_{-n}^{(1)} \right]_0 + \gamma K^2 [(\boldsymbol{v}^{(1)} \cdot \nabla)\boldsymbol{u}^{(1)}]_0 = -\nabla_s p_0^{(2)} + \Sigma \left(\partial_{zz}^2 \boldsymbol{u}_0^{(2)} + M \left[p^{(1)} \partial_{zz}^2 \boldsymbol{u}^{(1)} \right]_0 \right), \tag{33a}$$

$$\boldsymbol{u}_0^{(2)}\big|_{z=0} = [h^{(1)} \partial_z \boldsymbol{u}^{(1)}]_0, \quad \boldsymbol{u}_0^{(2)}\big|_{z=h^{(0)}} = 0, \tag{33b}$$

$$\bar{\boldsymbol{u}}_0^{(2)} = \frac{1}{h^{(0)}} \int_0^{h^{(0)}} \boldsymbol{u}_0^{(2)}\, dz - \left[\frac{h^{(1)}}{h^{(0)}} \bar{\boldsymbol{u}}^{(1)} \right]_0, \tag{33c}$$

where $[\cdot]_0$ corresponds to the zero harmonic of the expression (e.g., $[(p^{(1)})^2]_0 = p_1^{(1)} p_{-1}^{(1)} + p_1^{(-1)} p_1^{(1)}$).

The set of the first-order Eqs. (29), (30), and (31) and the set of the second-order Eqs. (32) and (33) together with the proper boundary conditions on $p^{(1)}$ and $p^{(2)}$ constitute the tool for computing the levitation force. The time-averaged force may be calculated by integrating the normal stress:

$$F_0 = -\iint \sigma_{zz}|_{z=h^{(0)}}\, dx_1\, dx_2 = \iint p_0^{(2)}\, dx_1\, dx_2. \tag{34}$$

F. Boundary conditions

The air flow inside the gap generates the flow outside. In order to keep the computational domain finite we have to replace the calculation of the outer flow by proper boundary conditions. The simplest way is to set pressure equal to its ambient value. However, such condition causes reflection of a longitudinal acoustic wave back into the gap and decreases the model accuracy. To avoid it we need special nonreflective boundary conditions. One of the first systematic studies of building such conditions was reported by Engquist and Majda [31]. For more details on the topic we refer the reader to Ref. [32].

In this section we derive a nonreflective boundary condition, which is transparent for acoustic wave. The idea is to find the relation between the pressure value and its gradient at the end of the gap. In order to do it, we need to consider the flow outside the gap. For simplicity, we assume that the vibrating surface and the levitating object are of the same size (e.g., having same radius in axisymmetric case).

1. First-order conditions

We employ the method suggested by Engquist and Majda [31]. In terms of their study, we use first approximation of the boundary conditions. It allows propagation of a nearly horizontal outgoing acoustic wave. The derivation of the conditions is described below.

Considering the infinite domain outside the gap, we start with the Navier-Stokes Eqs. (3a) and (3b). In contrast to the previous section, which described the flow in the gap, we cannot take advantage of the length scales ratio outside the gap. However, since the flow outside the gap is generated by the same vibration plane, we are still able to use the same series expansion on the small parameter ε and Fourier series in time. We continue to use the notation, introduced in the previous sections.

For the first order there is the system of equation in the nondimensional form:

$$\mathrm{i}n\gamma K^2 \boldsymbol{v}_n^{(1)} = -\nabla p_n^{(1)} + \Sigma_R \nabla \cdot \boldsymbol{\tau}_n^{(1)}, \tag{35a}$$

$$\mathrm{i}n\gamma^{-1} p_n^{(1)} + \nabla \cdot \boldsymbol{v}_n^{(1)} = 0, \tag{35b}$$

where $\Sigma_R = \mu_0 \omega / p_0$ is the squeeze number in the longitudinal direction and $\boldsymbol{\tau}_n^{(1)}$ is the nth harmonic of the first-order nondimensional viscous stress tensor:

$$\boldsymbol{\tau}_n^{(1)} = \left[\nabla \boldsymbol{v}_n^{(1)} + \left(\nabla \boldsymbol{v}_n^{(1)} \right)^T \right] + \left(\eta - \tfrac{2}{3} \right) \left(\nabla \cdot \boldsymbol{v}_n^{(1)} \right) \boldsymbol{I}, \tag{36}$$

where $\eta = \mu^b / \mu_0$ is the nondimensional bulk viscosity. The squeeze number Σ_R is small outside the gap (see Appendix), thus we can neglect the viscous terms in Eqs. (35a).

Taking the divergence of the Eqs. (35a) and utilizing the continuity Eq. (35b), one obtains that the pressure satisfies the following equation:

$$\nabla^2 p_n^{(1)} + K^2 n^2 p_n^{(1)} = 0, \tag{37}$$

where K is, as before, the nondimensional wave number.

As before, in the first-order, a nontrivial solution exists only for the harmonics with the number $n = \pm 1$.

After applying Fourier transform on z coordinate to Eq. (37) it takes the form

$$\nabla_s^2 \hat{p}_n^{(1)} + (K^2 n^2 - k^2) \hat{p}_n^{(1)} = 0, \tag{38}$$

where k is the Fourier space coordinate and $\hat{p}$ denotes the Fourier image of the pressure. The term in the brackets is denoted by B_n:

$$B_n = \sqrt{K^2 n^2 - k^2}. \tag{39}$$

Further, we examine two special cases of the geometry: the simplest 2D case and an axisymmetric case.

a. Nonaxisymmetric case. Here we investigate the simplest 2D nonaxisymmetric case. Equation (38) is read as

$$\frac{\partial^2 \hat{p}_n^{(1)}}{\partial x^2} + B_n^2 \hat{p}_n^{(1)} = 0. \tag{40}$$

The solution of Eq. (40) for the outgoing acoustic wave is given by

$$\hat{p}_n^{(1)} = \hat{p}_n^{(1)}\big|_{x=1} e^{\mathrm{i}B_n(x-1)}, \tag{41}$$

where $x = 1$ is the nondimensional coordinate of the levitating object's end. Note that if we do not neglect the viscous terms in Eq. (35), they will bring a small imaginary addition to B_n, which leads to attenuating of the acoustic wave as $x \to \infty$.

Although we do not know the exact pressure value at the end of the gap, we can find the relation between the pressure and its gradient:

$$\left.\frac{\partial \hat{p}_n^{(1)}}{\partial x}\right|_{x=1} = \mathrm{i}B_n\, \hat{p}_n^{(1)}\big|_{x=1}, \tag{42}$$

where $x = 1$ is denoted to the end of the gap.

The boundary condition Eq. (42) is given in the Fourier space. If we apply the inverse Fourier transform, the condition will be nonlocal in space. It is difficult to implement, so we need an approximation of the exact boundary condition Eq. (42). The most straightforward solution is to compute the coefficient on the right-hand side with $k = 0$. Physically, it means that we apply nonreflective boundary conditions to the horizontal waves only. In terms of Ref. [31] this is the first-order approximation of the boundary conditions. Since we do not have a pressure gradient in z direction inside the gap, such approximation is reasonable. Finally, we get the condition

$$\left.\frac{\partial p_n^{(1)}}{\partial x}\right|_{x=1} = \mathrm{i}K|n|\, p_n^{(1)}\big|_{x=1}. \tag{43}$$

b. Axisymmetric case. The idea described above can be applied to the axisymmetric case. The equation on the pressure outside the gap Eq. (38) takes the form

$$\frac{1}{r}\frac{\partial}{\partial r}\left(r\frac{\partial \hat{p}_n^{(1)}}{\partial r}\right) + B_n^2 \hat{p}_n^{(1)} = 0. \tag{44}$$

The outgoing wave for the case of the axisymmetric Helmholtz-type Eq. (44) is described by the Hankel function of the first kind $H_0^{(1)}$:

$$\hat{p}_n^{(1)} = \hat{p}_n^{(1)}\big|_{r=1} \frac{H_0^{(1)}(B_n r)}{H_0^{(1)}(B_n)}, \tag{45}$$

where $r = 1$ is the nondimensional radius of the levitating disk.

Using the same approach as in the 2D case we get the expression for the boundary condition:

$$\left.\frac{\partial p_n^{(1)}}{\partial r}\right|_{r=1} = -\,p_n^{(1)}\big|_{r=1} K|n| \frac{H_1^{(1)}(K|n|)}{H_0^{(1)}(K|n|)}. \tag{46}$$

2. *Second-order pressure condition*

Moving to the second-order boundary conditions, for zero harmonic there is no wave propagation at all (since it is time-independent originally), so speaking about a "nonreflective" condition is irrelevant. However, it is possible to write out the second-order equation for the pressure in the domain outside the gap and try to follow the same procedure as for the first order. Nonetheless, the resulting equation includes products of the first-order velocities, which must be found before, and it makes analysis impossible in practice. Therefore, we stay with the trivial boundary conditions for the second order:

$$p_0^{(2)}\big|_{r=1} = 0. \tag{47}$$

III. RESULTS AND DISCUSSION

We solved the equations derived in the previous section for the case of axisymmetric levitating disk. If the disk is planar the problem can be solved analytically. However, the analytical solution for the second-order quantities is too complex to be analyzed. Thus, we solve the problem numerically with COMSOL Multiphysics software.

In contrast to direct numerical simulation (see, for example, Ref. [25]), our approach helps to reduce the initial nonlinear transient problem Eqs. (3)–(8) to five linear PDEs with no time-dependence. Thus, it is more beneficial in terms of computational costs.

We use 2D axisymmetric formulation. In this case the air gap is represented by a rectangle. The computation consists of two successive steps. We start with solving the first-order Eqs. (29), (30a), and (31) with boundary condition Eqs. (30b) and (46). As we argued earlier, nontrivial first-order solution exists only for the wave numbers $n = \pm 1$. Since the $n = -1$ solution is complex conjugated to the $n = +1$ one, it is enough to solve equations for $n = +1$ only. The pressure $p_1^{(1)}$ does not depend on z coordinate, thus the gap-averaged continuity Eq. (29) can be solved on the surface of vibration source. Equations (29) and (30a) are coupled through averaged velocity Eq. (30c).

Next, the first-order solution is substituted into the second-order Eqs. (32) and (33a) with boundary condition Eqs. (33b) and (47). Again, the continuity Eq. (32) is solved on the boundary only.

Due to the form of the governing equations, the mesh size can be chosen independently in the longitudinal and transversal directions. This simplifies the mesh generation significantly in comparison with the full transient Navier-Stokes model, where one has to be very careful about the mesh size and the time step. We use a regular rectangular mesh with highly stretched elements.

Calculations were made for the air at normal conditions: ambient density $\rho_0 = 1.14\,\mathrm{kg/m^3}$, ambient pressure $p_0 = 1\,\mathrm{atm}$, ambient viscosity $\mu_0 = 1.81 \times 10^{-5}\,\mathrm{Pa\,s}$, ambient temperature $T_0 = 291.15\,\mathrm{K}$, Sutherland's constant $C = 120\,\mathrm{K}$, and adiabatic index $\gamma = 1.4$.

From the form of governing equations, it is clear that there are two mechanisms of near-field levitation: inertial (or acoustic) and viscous. Their importance is expressed by the acoustic wave number K and the squeeze number Σ. The ratio of the nondimensional quantities γK^2 and Σ, which occur in the Eqs. (26) and (27), is proportional to the squared ratio of the gap thickness to the acoustic boundary layer thickness,

$$\Pi = \frac{\gamma K^2}{\Sigma} = \frac{H_0^2 \omega \rho_0}{\mu_0} = 2\left(\frac{H_0}{\delta}\right)^2, \tag{48}$$

where $\delta = \sqrt{2\mu_0/(\omega\rho_0)}$ is acoustic boundary layer thickness [29]. In the case of air and vibrating frequency 20 kHz, its value is $\delta \approx 15\,\mu\mathrm{m}$. Therefore, when the gap thickness is large

enough, $\Pi \gg 1$, inertial terms dominate and acoustic models can be used; in the opposite case, when the gap is smaller than the boundary layer, $\Pi \ll 1$, only viscous effects are important and Reynolds equation may be applied. However, for the intermediate regimes, $\Pi \approx 1$, more involved model is needed.

Further, in this section we discuss the levitation force and provide comparison to the experimental measurements from previously published paper and our experiments. After demonstration of the model validation we introduce qualitative results on the pressure profile.

A. Levitation force

As was shown in the previous section, the levitation force can be computed as an integral of pressure. In general, the pressure distribution depends on many factors such as levitation height, disk radius, vibration amplitude and frequency, and gas properties. However, modeling shows that the result is highly sensitive to the vibration amplitude and the levitation height, and less affected by other parameters.

The theory includes vibration amplitude in the small parameter $\varepsilon = a/H_0$. This parameter is not involved in the governing equations and appears as a scaling factor only. It implies that for fixed gap thickness the pressure value is proportional to the squared amplitude. The levitation height, in contrast, enters into all the equations and thus deeply influences on the final pressure distribution.

1. Comparison to published data

In Ref. [25] the levitation distance is predicted by numerically solving full transient Navier-Stokes system. In addition, experiments are carried out using a 19.5-kHz acoustic source and various aluminum disks of different sizes. We use this paper to validate our model and compare our results to the full numerical model and published experimental data.

Figures 2 and 3 represent the dependence of the levitation height on the amplitude of vibration velocity for disk radii $R = 10$ mm and $R = 20$ mm, respectively. Each plot in a series corresponds to levitation height of a disk with thickness thk.

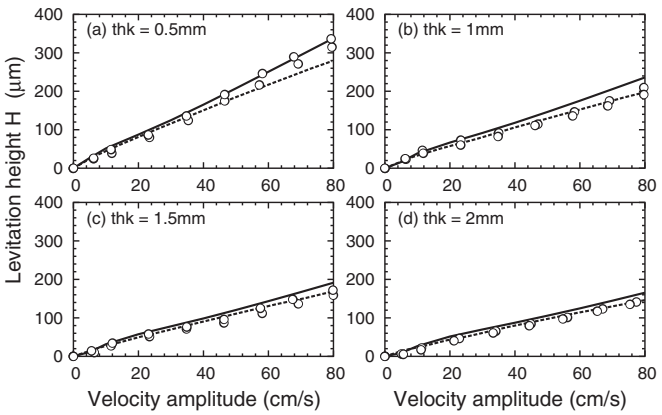

FIG. 2. Levitation height H as a function of the vibration velocity amplitude. Disk radius $R = 10$ mm, vibration frequency $f = 19.5$ kHz. Solid curves denote the present model; points represent the experimental data from Ref. [25]; and dashed lines correspond to numerical model from Ref. [25].

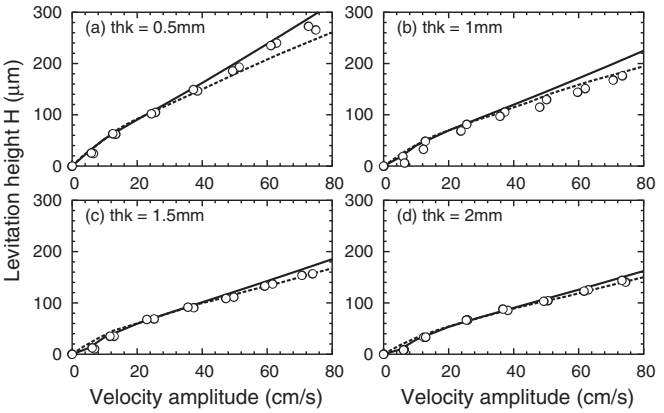

FIG. 3. Levitation height H as a function of the vibration velocity amplitude. Disk radius $R = 20$ mm, vibration frequency $f = 19.5$ kHz. Solid curves denote the present model; points represent the experimental data from Ref. [25]; and dashed lines correspond to numerical model from Ref. [25].

Both models—our semianalytical and published numerical one—are in good agreement with the experiment. However, our model has an advantage that it is much simpler for computation.

2. Comparison to the experiment

We have conducted a series of experiments in order to validate the model in various levitation regimes. During the experiments, the levitation height was measured for different aluminum and glass disks. The experimental setup is illustrated in Fig. 4. The transducer with piezos creates mechanical

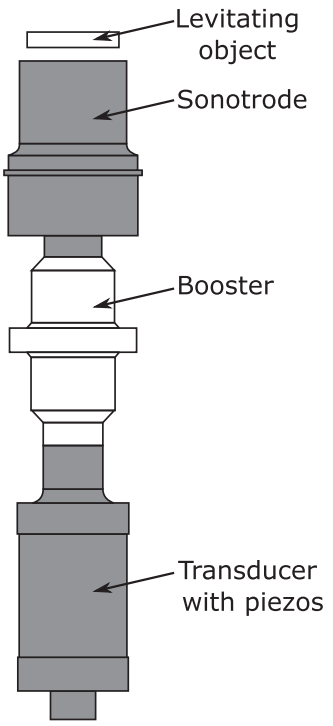

FIG. 4. Experimental setup.

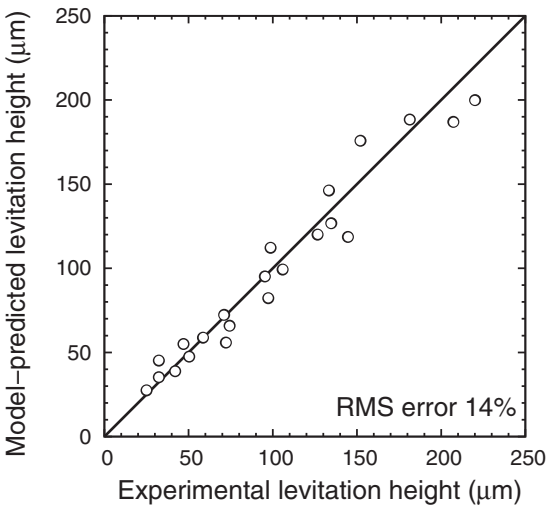

FIG. 5. Predicted levitation height vs. experimental data.

vibrations, which are amplified by the booster. The sonotrode on the top is designed to have a uniformly flat radiating face.

The transducer was run at 20 kHz and two vibration amplitudes were tested: 3 μm and 5 μm. Disks of radii 20 mm and 35 mm were used and the sample weight was in the range 3–200 g. The set of the experiments covered a wide range of levitation height from 26 μm to 220 μm. This allowed us to validate the model in both viscous and acoustic regimes. The summarized results are presented in Fig. 5, where the predicted levitation heights are compared to the experimental data. Our model agrees well with the experiment; the root-mean-square error over the set of experiments is 14%.

The dependence of the levitation height on the specific weight $\sigma = m/\pi R^2$ of the sample is shown in Fig. 6 in log-log scale. As described above, the change of vibration amplitude a results in shifting (i.e., scaling) the curves only. Also, the different radii almost do not affect the dependence. Furthermore, three regimes are observable. Each regime corresponds to a different slope of the curve on the plot. For the small levitation heights, less than about 20 μm, the viscous

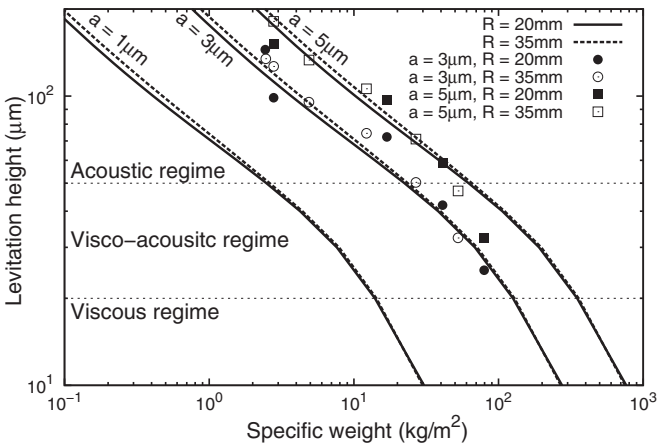

FIG. 6. Levitation height as a function of specific weight for different disk radii R and vibration amplitudes a. Points correspond to experimental data.

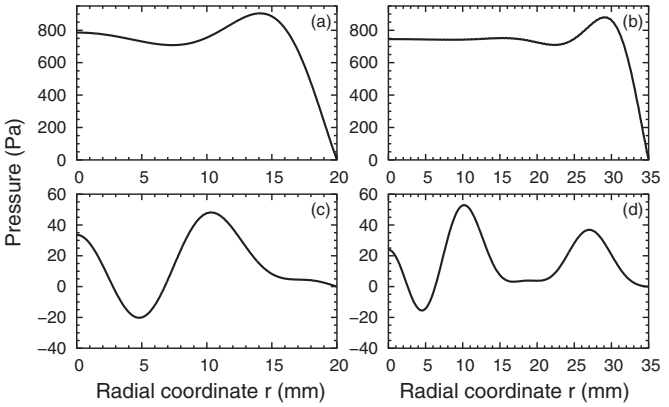

FIG. 7. Pressure profiles for various disk radii and levitation heights. Vibration amplitude $a = 3\,\mu$m for all cases. (a) $R = 20$ mm, $H = 30\,\mu$m; (b) $R = 35$ mm, $H = 30\,\mu$m; (c) $R = 20$ mm, $H = 150\,\mu$m; (d) $R = 35$ mm, $H = 150\,\mu$m.

regime works. It approximately corresponds to $\Pi < 3$. Then from 20 to 50 μm there is a viscoacoustic zone, where two mechanisms compete ($3 < \Pi < 20$). For the heights more than 50 μm acoustic effects dominate ($\Pi > 20$).

B. Pressure profile

Pressure profile may be important for some sensitive applications. Our model allows its computation. Modeling shows that the pressure distribution varies from almost uniform to wavy shape. As was discussed above, the key factor is the levitation height. For low heights, the boundary layers are overlapped and the system goes in viscous regime resulting in close-to-uniform pressure with a rapid drop near the edge only. In contrast, for larger heights, there is a distance between the boundary layers and inertia effects begin to play its role, which causes longitudinal acoustic wave and, therefore, a wavy pressure profile.

In Fig. 7, four different pressure profiles are illustrated. The plots in the first row correspond to viscous regime and show close-to-uniform distribution. On the other hand, the second row depicts the situation of acoustic regime, which creates a wavy profile. In addition, the pressure values indicate that the total levitation force significantly decreases in comparison with the viscous regime.

IV. CONCLUSION

In the present work, we derived an involved semianalytical model of ultrasonic near-filed levitation. In contrast to existing analytical models our approach does not require knowing the levitation height in advance and allows us to cover both viscous and acoustic regimes of levitation. Furthermore, the intermediate viscoacoustic regime is resolved. It is achieved by incorporation of multiple physical effects important in the process: inertia, viscosity, compressibility, viscosity-temperature-pressure dependence, nonplanar levitating object, and nontrivial boundary condition. Accounting for all these effects allows treating a wide range of levitation distances. At the same time, the model's accuracy is at the level of well-tuned straightforward numerical simulation. However,

due to reasonable assumptions and additional mathematical treatment the problem is reduced to five linear PDEs with no time-dependence. It implies low computational cost in comparison with the full numerical study.

During the model derivation we determined the applicability limits of the acoustic and viscous approaches and explained it in terms of the ratio of the gap thickness to the boundary layer thickness. The model results allow us to distinguish three regimes of the levitation, which show different change of levitation force with the gap thickness. In the case of small levitation distances, the boundary layers are overlapped and only viscous effects play a role. Then there is a viscoacoustic regime for moderate levitation heights, and, for large distances, the boundary layers are negligibly thin and inertial effects dominate. The last case allows propagation of the longitudinal acoustic wave, which results in a wavy pressure profile. Such waviness may be undesirable for highly sensitive levitating objects.

Although it was not in the focus of our work, the suggested approach allows study of acoustic streaming in the air gap. The steady flow is described by the second-order velocities $\boldsymbol{u}_0^{(2)}$, which are found from Eqs. (32)–(33a).

The model was successfully validated against the published experimental and numerical work of Nomura *et al.* [25]. In addition, a series of experiments was conducted to cover different levitation regimes. The model results are in good agreement with the experimental data with root-mean-square error of 14%.

ACKNOWLEDGMENTS

We are thankful to Thierry Dannoux, Ionel Lazer, and Pierre Brunello from Corning European Technology Center, Avon, France for their help with experiments. The work of Ivan Melikhov and Sergey Chivilikhin is partially financially supported by the Government of Russian Federation (Grant No. 074-U01) and by Grant No. 16-11-10330 of Russian Science Foundation.

APPENDIX: DETAILS OF SCALING ANALYSIS

1. Nondimensionalization

In this Appendix we describe how scaling analysis implies the transition form the initial Eqs. (3)–(8) to simplified Eqs. (11)–(15).

First of all, we reproduce the scaling used in the beginning of the Sec. II:

$$\tilde{x}_\alpha = \frac{x_\alpha}{R}, \quad \tilde{z} = \frac{z}{H_0}, \quad \tilde{t} = \omega t, \quad \tilde{v}_z = \frac{v_z}{\omega H_0}, \quad \tilde{v}_\alpha = \frac{v_\alpha}{\omega R},$$
$$\tilde{p} = \frac{p}{p_0}, \quad \tilde{\rho} = \frac{\rho}{\rho_0}, \quad \tilde{\mu} = \frac{\mu}{\mu_0}, \quad \tilde{s} = \frac{s}{c_v}, \quad \tilde{T} = \frac{T}{T_0},$$

where c_v is the heat capacity at constant volume and p_0, ρ_0, μ_0, T_0 are the pressure, density, viscosity, and temperature of air at normal conditions. Here and later Greek indices α, β, and φ span the numbers 1 and 2. The ratio of the gap thickness to the disk radius is denoted by $\zeta = H_0/R$. The second viscosity is nondimensionalized as $\eta = \mu^b/\mu_0$. The introduced length and velocity scales implies scaling of the viscous stress tensor,

$$\tilde{\tau}_{\alpha\beta} = \frac{\tau_{\alpha\beta}}{\mu_0\omega}, \quad \tilde{\tau}_{\alpha z} = \frac{H_0}{\mu_0\omega R}\tau_{\alpha z},$$
$$\tilde{\tau}_{z\alpha} = \frac{H_0}{\mu_0\omega R}\tau_{z\alpha}, \quad \tilde{\tau}_{zz} = \frac{\tau_{zz}}{\mu_0\omega},$$

the viscous dissipation term,

$$\tilde{\Phi} = \frac{H_0^2}{\mu_0\omega^2 R^2}\Phi,$$

and the total stress in z direction,

$$\tilde{\sigma}_{zz} = p_0\sigma_{zz}.$$

To simplify the notation we omit tildes over nondimensional variables.

The stress tensor components can be expressed in terms of velocities:

$$\tau_{\alpha\beta} = \mu\left(\frac{\partial v_\alpha}{\partial x_\beta} + \frac{\partial v_\beta}{\partial x_\alpha}\right) + \left(\eta - \frac{2}{3}\mu\right)\left(\frac{\partial v_\varphi}{\partial x_\varphi} + \frac{\partial v_z}{\partial z}\right)\delta_{\alpha\beta}, \tag{A1}$$

$$\tau_{\alpha z} = \tau_{z\alpha} = \mu\left(\frac{\partial v_\alpha}{\partial z} + \zeta^2\frac{\partial v_z}{\partial x_\alpha}\right), \tag{A2}$$

$$\tau_{zz} = 2\mu\frac{\partial v_z}{\partial z} + \left(\eta - \frac{2}{3}\mu\right)\left(\frac{\partial v_\varphi}{\partial x_\varphi} + \frac{\partial v_z}{\partial z}\right), \tag{A3}$$

where $\delta_{\alpha\beta}$ is Kronecker δ and summation over repeated Greek indices is assumed. Then the viscous dissipation term Φ may be written as

$$\Phi = \tau_{\alpha z}\frac{\partial v_\alpha}{\partial z} + \zeta^2\left(\tau_{\alpha\beta}\frac{\partial v_\alpha}{\partial x_\beta} + \tau_{z\alpha}\frac{\partial v_z}{\partial x_\alpha} + \tau_{zz}\frac{\partial v_z}{\partial z}\right). \tag{A4}$$

After nondimensionalization momentum Eqs. (3a) take the form

$$\gamma K^2\rho\left(\frac{\partial v_\alpha}{\partial t} + v_\beta\frac{\partial v_\alpha}{\partial x_\beta} + v_z\frac{\partial v_\alpha}{\partial z}\right) = -\frac{\partial p}{\partial x_\alpha} + \Sigma\left(\frac{\partial \tau_{\alpha z}}{\partial z} + \zeta^2\frac{\partial \tau_{\alpha\beta}}{\partial x_\beta}\right), \tag{A5}$$

$$\gamma\zeta^2 K^2\rho\left(\frac{\partial v_z}{\partial t} + v_\beta\frac{\partial v_z}{\partial x_\beta} + v_z\frac{\partial v_z}{\partial z}\right) = -\frac{\partial p}{\partial z} + \zeta^2\Sigma\left(\frac{\partial \tau_{z\beta}}{\partial x_\beta} + \frac{\partial \tau_{zz}}{\partial z}\right), \tag{A6}$$

where nondimensional numbers K and Σ are defined as

$$K = \sqrt{\frac{\omega^2 R^2\rho_0}{\gamma p_0}}, \quad \Sigma = \frac{\mu_0\omega R^2}{p_0 H_0^2}.$$

The continuity Eq. (3b) takes the nondimensional form

$$\frac{\partial\rho}{\partial t} + \frac{\partial}{\partial x_\alpha}(\rho v_\alpha) + \frac{\partial}{\partial z}(\rho v_z) = 0. \tag{A7}$$

The energy Eq. (6) is written as

$$\rho T\left(\frac{\partial s}{\partial t} + v_\alpha\frac{\partial s}{\partial x_\alpha} + v_z\frac{\partial s}{\partial z}\right) = \Lambda\left(\frac{\partial^2 T}{\partial z^2} + \zeta^2\frac{\partial^2 T}{\partial x_\alpha\partial x_\alpha}\right) + \Theta\Phi, \tag{A8}$$

where nondimensional numbers Λ and Θ are defined as

$$\Lambda = \frac{\kappa}{\rho_0 \omega c_v H_0^2}, \quad \Theta = \frac{\mu_0 \omega R^2}{\rho_0 c_v T_0 H_0^2}. \tag{A9}$$

Finally, the total stress in z direction, which is used for computation of levitation force, is

$$\sigma_{zz} = -p + \zeta^2 \Sigma \tau_{zz}. \tag{A10}$$

2. Neglecting small terms

For further analysis we will need the following relationships, which may be found in Refs. [29,33]:

$$c = \sqrt{\gamma \frac{\mathcal{R} T_0}{\mathcal{M}}} = \sqrt{\gamma \frac{p_0}{\rho_0}}, \quad \bar{c} = \sqrt{\frac{8 \mathcal{R} T_0}{\pi \mathcal{M}}} = \sqrt{\frac{8}{\pi \gamma}} c$$

$$\mu_0 = \frac{\rho_0 l \bar{c}}{3}, \quad \kappa = \frac{\rho_0 l \bar{c}}{3} c_v,$$

$$c_p - c_v = \mathcal{R}/\mathcal{M}, \quad c_p/c_v = \gamma,$$

where c is the speed of sound, $\bar{c}$ is the mean molecular speed, l is the molecular mean-free path, $\mathcal{R}$ is the universal gas constant, $\mathcal{M}$ is the molar mass of gas, and c_v and c_p are specific heat capacities at constant volume and constant pressure, respectively.

Next we use the introduced relationships to estimate magnitudes of the nondimensional numbers K, Σ, Λ, Θ. Assuming the typical disk radius $R \sim 10^{-2}$ m, gap thickness $H_0 \sim 10^{-5}$–10^{-4} m, acoustic wavelength $\lambda \sim 10^{-2}$ m, vibration amplitude $a \sim 10^{-6}$ m, and mean-free path $l \sim 10^{-8}$ m, we obtain the characteristic values:

$$\zeta = \frac{H_0}{R} \sim 10^{-3} - 10^{-2},$$

$$\varepsilon = \frac{a}{H_0} \sim 10^{-2} - 10^{-1},$$

$$K = 2\pi \frac{R}{\lambda} \sim 10^0,$$

$$\gamma K^2 = 4\pi^2 \gamma \frac{R^2}{\lambda^2} \sim 10^1,$$

$$\gamma \zeta^2 K^2 = 4\pi^2 \gamma \frac{H_0^2}{\lambda^2} \sim 10^{-5} - 10^{-3},$$

$$\Sigma = \frac{4\sqrt{2\pi\gamma}}{3} \frac{l R^2}{\lambda H_0^2} \sim 10^{-2} - 10^0,$$

$$\zeta^2 \Sigma = \frac{4\sqrt{2\pi\gamma}}{3} \frac{l}{\lambda} \sim 10^{-6},$$

$$\Lambda = \frac{\sqrt{2}}{3\pi\sqrt{\pi\gamma}} \frac{l\lambda}{H_0^2} \sim 10^{-4} - 10^{-2},$$

$$\Theta = (\gamma - 1)\Sigma \sim 10^{-2} - 10^0.$$

Basing on the estimated values, we can neglect the terms involving $\gamma \zeta^2 K^2$, $\zeta^2 \Sigma$, and Λ. The numbers γK^2 and Σ cannot be neglected.

We will pay a special attention to the quantity Θ. Though it is of the same order as Σ, detailed analysis shows that the term $\Theta\Phi$ of Eq. (A8) can be omitted.

First of all, we should note that the viscous dissipation term Φ is quadratic in the velocity amplitude. Due to Eqs. (A2) and (A4) in the leading order, it has the form

$$\Theta\Phi = \Theta\mu \frac{\partial v_\alpha}{\partial z} \frac{\partial v_\alpha}{\partial z}. \tag{A11}$$

It does not affect the equations of first order in ε. Consequently, in the first order we have

$$\frac{\partial s^{(1)}}{\partial t} = 0. \tag{A12}$$

Then we recall the first-order analysis described in the paper. For the case of a planar axisymmetric disk, the first-order Eqs. (29) and (30) can be solved analytically, giving

$$v_1^{(1)} = -\frac{\mathrm{i}}{\gamma K^2} \left(\frac{\sinh(\varkappa z) \sinh(\varkappa(1-z))}{\sinh(\varkappa)} - 1 \right) \frac{\partial p_1^{(1)}}{\partial r}, \tag{A13}$$

$$p_1^{(1)} = \frac{\gamma}{2} \left(1 - \frac{K J_0(rk)}{K J_0(k) - \mathrm{i} k J_1(k)} \right), \tag{A14}$$

where v is the radial velocity, p is the pressure,

$$\varkappa = \sqrt{\mathrm{i}\Pi} = \sqrt{\mathrm{i}\frac{\gamma K^2}{\Sigma}}, \quad k = \frac{\omega R}{c\sqrt{1 - 2\varkappa^{-1} \tanh(\varkappa/2)}},$$

and J_0, J_1 are zero- and first-order Bessel functions of the first kind.

We will examine the velocity derivative $\partial v/\partial z$ in the limiting viscous and acoustic regimes. It takes the largest value on the boundary. For the viscous case $\varkappa \ll 1$ the asymptotic relation holds

$$\max \left| \frac{\partial v_1^{(1)}}{\partial z} \right| \sim \left| \frac{\varkappa^2}{2\gamma K^2} \frac{\partial p_1^{(1)}}{\partial r} \right| = \frac{1}{2\Sigma} \left| \frac{\partial p_1^{(1)}}{\partial r} \right|. \tag{A15}$$

To estimate the pressure gradient we note that $k \sim \varkappa^{-1}$ and employ the Bessel function asymptotic for large arguments [34]. It leads to the magnitude approximation

$$\left| \frac{\partial p_1^{(1)}}{\partial r} \right| \sim \frac{\gamma K}{2}. \tag{A16}$$

Substituting estimations (A15) and (A16) into Eq. (A11), we obtain

$$\Theta\Phi = \Theta\varepsilon^2 \left| \frac{\partial v_1^{(1)}}{\partial z} \right|^2 \sim \epsilon^2 \frac{\gamma^2(\gamma-1)K^2}{16\Sigma}$$

$$= \frac{3\gamma^2(\gamma-1)\pi^2}{16\sqrt{(2\pi\gamma)}} \frac{a^2}{l\lambda} \sim 10^{-3}. \tag{A17}$$

Therefore, for viscous regime the right side of the energy Eq. (A8) vanishes.

Similar analysis for acoustic regime, $\varkappa \gg 1$, gives estimations

$$\max \left| \frac{\partial v_1^{(1)}}{\partial z} \right| \sim \left| \frac{\varkappa}{\gamma K^2} \frac{\partial p_1^{(1)}}{\partial r} \right| = \frac{1}{K\sqrt{\gamma\Sigma}} \left| \frac{\partial p_1^{(1)}}{\partial r} \right|, \tag{A18}$$

$$\left| \frac{\partial p_1^{(1)}}{\partial r} \right| \sim \frac{\gamma K}{2}, \tag{A19}$$

resulting in the typical scale of viscous dissipation term

$$\Theta\Phi = \Theta\varepsilon^2 \left| \frac{\partial v_1^{(1)}}{\partial z} \right|^2 \sim \epsilon^2 \frac{\gamma(\gamma-1)}{4} = \frac{\gamma(\gamma-1)}{4} \frac{a^2}{H_0^2} \sim 10^{-5}. \quad \text{(A20)}$$

The estimated magnitudes of the viscous dissipation term for viscous case Eq. (A17) and acoustic case Eq. (A20) allows us to neglect it in our calculations.

In addition, the magnitude of $\Theta\Phi$ was computed with the exact first-order solution Eqs. (A13) and (A14) numerically for the heights 10–200 μm and disk radii 5–50 mm. The calculations confirm that viscous dissipation term is negligible comparing to ε^2 and thus can be omitted.

3. Simplified equation

Summarizing the scaling analysis of the former section we end up with the following simplified momentum equations:

$$\gamma K^2 \rho[\partial_t \boldsymbol{u} + (\boldsymbol{v}\cdot\boldsymbol{\nabla}\boldsymbol{u})] = -\boldsymbol{\nabla}_s p + \Sigma\partial_z(\mu\partial_z \boldsymbol{u}), \quad \text{(A21)}$$

$$\partial_z p = 0, \quad \text{(A22)}$$

continuity equation

$$\partial_t \rho + \boldsymbol{\nabla}\cdot(\rho\boldsymbol{v}) = 0, \quad \text{(A23)}$$

and energy equation

$$\partial_t s + \boldsymbol{v}\cdot\boldsymbol{\nabla} s = 0. \quad \text{(A24)}$$

The total stress in z direction is reduced to

$$\sigma_{zz} = -p. \quad \text{(A25)}$$

These simplified equations are used in the main body of the paper.

[1] E. O. J. Salbu, J. Basic Eng. **86**, 355 (1964).
[2] Y. Hashimoto, Y. Koike, and S. Ueha, J. Acoust. Soc. Am. **100**, 2057 (1996).
[3] Y. Hashimoto, Y. Koike, and S. Ueha, J. Acoust. Soc. Am. **103**, 3230 (1998).
[4] S. Ueha, Y. Hashimoto, and Y. Koike, Ultrasonics **38**, 26 (2000).
[5] T. Ide, J. Friend, K. Nakamura, and S. Ueha, Sens. Actuators, A **135**, 740 (2007).
[6] S. Yoshimoto, Y. Anno, Y. Sato, and K. Hamanaka, JSME Int. J., Ser. C **40**, 353 (1997).
[7] S. Yoshimoto, H. Kobayashi, and M. Miyatake, Tribol. Int. **40**, 503 (2007).
[8] J. Hu, K. Nakamura, and S. Ueha, Ultrasonics **35**, 459 (1997).
[9] K.-T. Chang, Ultrasonics **43**, 49 (2004).
[10] C. Wang and Y. H. J. Au, Int. J. Adv. Manufact. Technol. **60**, 1 (2011).
[11] S. Zhao, S. Mojrzisch, and J. Wallaschek, Mech. Syst. Sig. Process. **36**, 168 (2013), piezoelectric Technology.
[12] L. Rayleigh, Philosophical Magazine Series 6, **3**, 338 (1902).
[13] L. Rayleigh, Philosophical Magazine Series 6, **10**, 364 (1905).
[14] B. Chu and R. E. Apfel, J. Acoust. Soc. Am. **72**, 1673 (1982).
[15] C. P. Lee and T. G. Wang, J. Acoust. Soc. Am. **94**, 1099 (1993).
[16] M. Settnes and H. Bruus, Phys. Rev. E **85**, 016327 (2012).
[17] P. B. Muller and H. Bruus, Phys. Rev. E **90**, 043016 (2014).
[18] P. B. Muller, M. Rossi, A. G. Marín, R. Barnkob, P. Augustsson, T. Laurell, C. J. Kähler, and H. Bruus, Phys. Rev. E **88**, 023006 (2013).
[19] J. T. Karlsen and H. Bruus, Phys. Rev. E **92**, 043010 (2015).
[20] S. A. Chivilikhin, A. S. Amosov, and I. F. Melikhov, Nanosyst.: Phys. Chem. Math. **4**, 592 (2013).
[21] B. Hamrock, S. Schmid, and B. Jacobson, *Fundamentals of Fluid Film Lubrication*, Mechanical Engineering (CRC Press, Boca raton, FL, 2004).
[22] A. Minikes and I. Bucher, J. Sound Vib. **263**, 241 (2003).
[23] A. Minikes, I. Bucher, and S. Haber, J. Acoust. Soc. Am. **116**, 217 (2004).
[24] D. Ilssar and I. Bucher, J. Sound Vib. **354**, 154 (2015).
[25] H. Nomura, T. Kamakura, and K. Matsuda, J. Acoust. Soc. Am. **111**, 1578 (2002).
[26] A. Minikes and I. Bucher, J. Fluids Struct. **22**, 713 (2006).
[27] S. R. Turns, J. Lubr. Technol. **105**, 361 (1983).
[28] J. Li, W. Cao, P. Liu, and H. Ding, Appl. Phys. Lett. **96**, 243507 (2010).
[29] L. D. Landau and E. M. Lifshitz, *Fluid Mechanics*, 2nd ed., Vol. 6 (Pergamon Press, Oxford, 1993).
[30] W. Sutherland, Philosophical Magazine Series 5, **36**, 507 (1893).
[31] B. Engquist and A. Majda, Math. Comput. **31**, 629 (1977).
[32] D. Givoli, J. Comput. Phys. **94**, 1 (1991).
[33] A. Sommerfeld, *Lectures on Theoretical Physics: Thermodynamics and Statistical Mechanics*, edited by F. Bopp, J. Meixner, and J. Kestin (Academic Press, New York, 1964).
[34] M. Abramowitz and I. A. Stegun, *Handbook of Mathematical Functions with Formulas, Graphs, and Mathematical Tables* (Wiley-Interscience, New York, 1984).